HAL open science

The pathogenic MT-ATP6 m.8851T>C mutation prevents proton movements within the n-side hydrophilic cleft of the membrane domain of ATP synthase

Alain Dautant, Roza Kucharczyk, Kewin Gombeau, François Godard, Déborah Tribouillard-Tanvier, Jean-Paul Di Rago

To cite this version:

Alain Dautant, Roza Kucharczyk, Kewin Gombeau, François Godard, Déborah Tribouillard-Tanvier, et al.. The pathogenic MT-ATP6 m.8851T>C mutation prevents proton movements within the n-side hydrophilic cleft of the membrane domain of ATP synthase. Biochimica biophysica acta (BBA) - Bioenergetics, 2019, 1860 (7), pp.562-572. 10.1016/j.bbabio.2019.06.002 . hal-02988559

HAL Id: hal-02988559

https://cnrs.hal.science/hal-02988559v1

Submitted on 25 Oct 2021

HAL is a multi-disciplinary open access archive for the deposit and dissemination of scientific research documents, whether they are published or not. The documents may come from teaching and research institutions in France or abroad, or from public or private research centers.

L'archive ouverte pluridisciplinaire **HAL**, est destinée au dépôt et à la diffusion de documents scientifiques de niveau recherche, publiés ou non, émanant des établissements d'enseignement et de recherche français ou étrangers, des laboratoires publics ou privés.

Distributed under a Creative Commons Attribution - NonCommercial 4.0 International License

Version of Record: https://www.sciencedirect.com/science/article/pii/S0005272819300544
Manuscript_f615058fbcf6d53647c3a09fcad9a4c9

The pathogenic *MT-ATP6* m.8851T>C mutation prevents proton movements within the *n*-side hydrophilic cleft of the membrane domain of ATP synthase

Roza Kucharczyk[1, 2, a,*], Alain Dautant[1, a], Kewin Gombeau[1], François Godard[1], Déborah Tribouillard-Tanvier[1, $], and Jean-Paul di Rago[1, *]

[1] Institut de Biochimie et Génétique Cellulaires of CNRS, Bordeaux University, 1 Rue Camille Saint-Saëns, Bordeaux 33077 cedex, France.

[2] Institute of Biochemistry and Biophysics, Polish Academy of Sciences, Warsaw, Poland

[a] These authors equally contributed to this work

[$] Research Associate from INSERM

*To whom correspondence should be addressed. Email : jp.dirago@ibgc.cnrs.fr or roza@ibb.waw.pl

© 2019 published by Elsevier. This manuscript is made available under the CC BY NC user license
https://creativecommons.org/licenses/by-nc/4.0/

Abstract

Dozens of pathogenic mutations have been localized in the mitochondrial gene (*MT-ATP6*) that encodes the subunit *a* of ATP synthase. The subunit *a* together with a ring of identical subunits *c* moves protons across the mitochondrial inner membrane coupled to rotation of the subunit *c*-ring and ATP synthesis. One of these mutations, m.8851T>C, has been associated with bilateral striatal lesions of childhood (BSLC), a group of rare neurological disorders characterized by symmetric degeneration of the corpus striatum. It converts a highly conserved tryptophan residue into arginine at position 109 of subunit *a* ($aW_{109}R$). We previously showed that an equivalent thereof in *Saccharomyces cerevisiae* ($aW_{126}R$) severely impairs by an unknown mechanism the functioning of ATP synthase without any visible assembly/stability defect. Herein we show that ATP synthase function was recovered to varying degree by replacing the mutant arginine residue 126 with methionine, lysine or glycine or by replacing with methionine an arginine residue present in position 169 of subunit *a* (aR_{169}). In recently described atomic structures of yeast ATP synthase, aR_{169} is at the center of an hydrophilic cleft along which protons are transported from the subunit *c*-ring to the mitochondrial matrix, in the proximity of the two residues known from a long time to be essential to the activity of F_O (aR_{176} and cE_{59}). We provide evidence that the $aW_{126}R$ change is responsible for an electrostatic and steric hindrance that enables aR_{169} to engage in a salt bridge with cE_{59}. As a result, aR_{176} cannot interact properly with cE_{59} and ATP synthase fails to effectively move protons across the mitochondrial membrane. In addition to insight into the pathogenic mechanism induced by the m.8851T>C mutation, the present study brings interesting information on the role of specific residues of subunit *a* in the energy-transducing activity of ATP synthase.

Introduction

Mitochondria provide aerobic eukaryotes with cellular ATP through the process of oxidative phosphorylation (OXPHOS) [1]. In this process electrons released by the oxidation of fatty acids and carbohydrates are shuttled to oxygen by four complexes (I–IV) embedded in the mitochondrial inner membrane and protons are concomitantly transported from the mitochondrial matrix into the space between the two membranes that surround the organelle. Protons are returned back to the matrix by ATP synthase (complex V), which is coupled to ATP synthesis from ADP and inorganic phosphate [2]. The ATP synthase organizes into a membrane-embedded domain (F_O) and a membrane-extrinsic catalytic sector (F_1) [3-5]. Within the F_O, protons are transported by the subunit *a* and a ring of identical *c* subunits (8 in mammals, 10 in yeast [6]), which leads to rotation of the subunit *c*-ring and conformational changes in the F_1 that favor the synthesis of ATP and its release into the mitochondrial matrix.

Considerable progress towards a molecular description of the energy-transducing mechanism of ATP synthase has been achieved recently with the resolution of complete atomic structures of this enzyme [4, 7-9]. Evaluating the role of specific amino acid residues in these structures requires a genetically approachable system where nuclear and mitochondrial genes can be modified because of the mixed genetic origin of ATP synthase in the vast majority of eukaryotes. Baker's yeast *Saccharomyces cerevisiae* is by far the most convenient [10]. The incapacity of cells from this unicellular fungus to stably maintain the co-existence of different mitochondrial DNA molecules (heteroplasmy) is especially helpful to investigate in isolation the functional consequences of specific mutations of this DNA [11]. Another major advantage is the good fermenting capacity of *S. cerevisiae*, which enables survival to mutations that inactivate oxidative phosphorylation.

We have exploited these attributes to investigate the biochemical consequences of pathogenic amino acid replacements in subunit *a* induced by mutations in the mitochondrial *MT-ATP6* gene [12-18]. With yeast strains homoplasmic for equivalents of these mutations it was possible to evaluate more precisely their impact on ATP synthase than with patient's cells and tissues where they generally co-exist with wild type mtDNA (heteroplasmy). In all cases a substantial lack of mitochondrial ATP production, ranging from 30 to >90%, was observed in correlation with the severity of the clinical

phenotypes induced by these mutations. Although interesting, these observations provide limited information because detrimental amino acid changes may affect residues that have minor if any functional importance. However, one can take advantage of loss-of-function mutations to seek for genetic reversions that lead to function regain without recovering the wild type structure of subunit *a*, an approach that proved to be highly informative on several occasions. For instance, we recently provided in this way evidence that a pathogenic serine-to-asparagine change at position 165 of yeast subunit *a* (148 in humans) prevents the transport of protons from the subunit *c*-ring to the mitochondrial matrix [18] not because the mutated serine is directly involved in proton conduction but because its replacement by asparagine leads to the establishment of hydrogen bonds with a nearby glutamate residue (aE_{162}) that is important for moving protons through the F_O [19].

We herein applied this suppressor genetics approach to the m.8851T>C mutation that has been associated to bilateral striatal lesions of childhood (BSLC), a group of rare neurological disorders characterized by symmetric degeneration of the corpus striatum [20]. This mutation leads to replacement of a highly conserved tryptophan residue with arginine at position 109 of human subunit *a* ($aW_{109}R$). An equivalent thereof ($aW_{126}R$) very severely compromises the ability of yeast to proliferate from non-fermentable substrates (e.g. glycerol, ethanol, or lactate) owing to defects in the functioning of F_O without any visible impact on the assembly/stability of ATP synthase [15]. We here report that ATP synthase function was recovered to varying degrees by replacing the mutant arginine residue 126 with methionine, lysine or glycine or by replacing with methionine an arginine residue present in position 169 of subunit *a* (aR_{169}). The results provide evidence that the m.8851T>C mutation impairs the movement of protons from the subunit *c*-ring towards the mitochondrial matrix owing to electrostatic and steric hindrance with residues essential to the activity of F_O [7, 21].

2. Materials and Methods

2.1. *Growth media*

The media used for growing yeast were: YPGA (1% Bacto yeast extract, 1% Bacto Peptone, 2% or 10% glucose, 40 mg/L adenine); YPGalA (1% Bacto yeast extract, 1% Bacto Peptone, 2% galactose, 40 mg/L adenine); YPEGA (1% Bacto yeast extract, 1% Bacto Peptone, 3% ethanol, 2% glycerol, 40 mg/L adenine); W0 (2% glucose, 0.67% Nitrogen base with ammonium sulfate from Difco). Sporulation was induced in SP1 medium: 0.1% glucose, 0.25% yeast extract, and 50 mM potassium acetate. Solid media were obtained by adding 2% Bacto Agar (Difco, Becton Dickinson).

2.2. *Selection of revertants from strain RKY39 (aW_{126}R).*

The strain RKY39 (*MAT**a** ade2-1 his3-11,15 trp1-1 leu2-3,112 ura3-1 CAN1 arg8::HIS3* [ρ^+ *atp6-W_{126}R*]) that carries an equivalent of the m.8851T>C (*a*W_{126}R) mutation [15] was subcloned on rich 2% glucose plates. Forty subclones were picked up and individually grown for three days in 10% glucose. Glucose was removed from the cultures by two washings with water and 10^8 cells from each culture were spread on rich glycerol/ethanol (YPEGA) plates. The plates were incubated at 28°C for at least fifteen days. Only one revertant per plate was retained for further analysis to ensure genetic independence of the isolates. The revertants were genetically purified by subcloning on glucose plates and their *ATP6* gene was PCR-amplified with primers 5'TAATATACGGGGGTGGGTCCCTCAC and 5'GGGCCGAACTCCGAAGGAGTAAG and entirely sequenced.

2.3 Epifluorescence Microscopy. Epifluorescence microscopy of 4',6-diamidino-2-phenylindole (DAPI)-stained and MitoTracker-Red CMXRos-stained cells was carried out with a Zeiss AxioImager A2 microscope fitted with a ×100 immersion objective and a standard FITC filter. Briefly, 3mL of log-phase culture were incubated with DAPI (5µg.mL^{-1}) and Mitotracker CMX ROS (1µg.mL^{-1}) for 10min at 28°C with agitation. Then, cells were washed with 10mL of minimal media to remove the excess of flurochrome, centrifugated and resuspended in 100µL of minimal media prior to be observed.

Yeast RNA preparation and quantitative real-time PCR assay. For each condition, a cellular equivalent of 5 OD_{600nm} was sampled in log-phase culture grown for 8h in rich galactose media and quick frozen to be further processed for total RNA extraction. To this aim, the Absolutely RNA Miniprep kit (Agilent, Stratagene) was used, according to the manufacturer's instructions with the following modification: to 300 µL of the lysis buffer containing guanidine thiocyanate and 2.1 µL β-mercaptoethanol were subsequently added an equal volume of glass beads (Ø 0.5 mm) and an equal volume of phenol:chloroform:isoamyl alcohol (25:24:1). Cells were then disrupted by vortexing 5 times for 30 seconds with station of 30 seconds in ice between each vortex session to avoid excessive warming. The elution volume was 30 µL and the concentration of RNA was quantified using a nanodrop spectrometer (NanoDrop 1000, Thermo Scientific). RNA purity was checked and met the following requirements: A260/A280 >1.7 and A260/A230 >1.5. The integrity of the 18 and 26S ribosomal bands was checked on a 1% agarose gel. First-strand cDNA was synthesized from 500 ng total RNAs using the Affinity script QPCR cDNA synthesis kit (Agilent, Stratagene) according to the manufacturer's instructions. The retro-transcription was performed by incubating the reactions at 25°C for 5 min, 42°C for 45 min, and 95°C for 5 min. Specific primer pairs were determined using Primer-BLAST software [22] and matched the coding sequence of the target genes. The GenBank accession numbers and the corresponding primer pairs are summarised in Table S1. Real-time qPCR reactions were performed using a Mx3000P QPCR System (Agilent, Stratagene) and the Brillant III Ultra-Fast SYBR® Green QPCR Master Mix with Low ROX (Agilent, Stratagene) according to the marnufacturer’s instructions. The programme used was: one cycle at 95°C for 3 min and then 40 amplification cycles at 95°C for 20 sec and 60°C for 20 sec. For each sample, the level of expression of the target gene was compared to the expression of the stably expressed *TFC6*, *TFB1* and *RMD8* genes. That relative expression (REX) of the target gene was calculated according to the formula REX = $\mathrm{MEAN}[(E_{TFC6})^{\mathrm{Ct}\text{-}TFC6} + (E_{TFB1})^{\mathrm{Ct}\text{-}TFB1} + (E_{RMD8})^{\mathrm{Ct}\text{-}RMD8}]/(E_{target})^{\mathrm{Ct}\text{-}target}$. Ct is the number of PCR cycles needed to enter in exponential phase of amplification; E is the amplification efficiency of couples of primers specific to the reference and target genes, respectively. For each gene, the mean value of the relative expression level, and the associated standard error (n = 3) were determined. Standard curves were generated using 10-fold dilutions of a cDNA template on the Mx3000P apparatus, and using

each couple of gene specific primers (one standard curve per couple). Each dilution was assayed in duplicate for each couple of primers. The reaction specificity was determined for each reaction from the dissociation curve of the PCR product. This dissociation curve was obtained by following the SybrGreen fluorescence level during a gradual heating of the PCR products from 55 to 95°C. Samples were run in duplicate in optically clear 96-well plates (Agilent, Stratagene). All qPCR experiments were performed according to the MIQE (Minimum Information for publication of Quantitative real-time PCR Experiments) guidelines [23]. Each standard curve was made by plotting the Ct against the log of the starting quantity of template for each dilution. The equation for the regression line and the r-value was calculated. From that equation the slope of the standard curve was deduced and used to calculate the PCR efficiency, E, for each couple of primers, as follows: $E = 10^{-1}/\text{slope}$. The measured hybridization efficiencies were 1.85, 1.92, 1.89, 1,84 and 1.83 for *TFC6*, *TFB1*, *RMD8*, *COX2* and *ATP8* genes, respectively.

2.4 Quantification of mitochondrial DNA copy number per cell. Measurement of mitochondrial DNA copy number was determined using a previously described method [24]. For each condition, a cellular equivalent of 1 OD_{600nm} was sampled in log-phase culture grown for 8h in rich galactose media and quick frozen to be further processed for total DNA extraction. Total DNA was extracted as described in Venegas and Halberg (2012) with minor modifications. Briefly, cells were lysed in 100 µL LiAc 0,2M SDS 1% at 75°C for 10min, then mixed with 300 µl 100% EtOH and centrifugated for 3min at 15000g followed by a washing step with 500µL 70% EtOH and centrifugated for 3min at 1500g. Finally, total DNA was resuspended in 100µL TE (Tris 10mM pH8; EDTA 1mM) and 1µL of a 10-fold dilution used as template for RT-qPCR measurement. The GenBank accession numbers and the corresponding primer pairs are summarised in Table S1 (same primer pairs used for gene expression analysis). Real-time qPCR reactions were performed using a Mx3000P QPCR System (Agilent, Stratagene) and the Brillant III Ultra-Fast SYBR® Green QPCR Master Mix with Low ROX (Agilent, Stratagene) according to the marnufacturer's instructions. The programme used was: one cycle at 95°C for 3 min and then 40 amplification cycles at 95°C for 20 sec and 60°C for 20 sec. For each sample, the mitochondrial DNA copy-number (MtDNA copy

number) was determined by comparing the abundance of a single-copy nuclear gene (*TFB1*) relatively to that of the mitochondrially-encoded gene *COX2* using the following formula: MtDNA copy number = $(E_{TFB1})^{Ct\text{-}TFB1} / (E_{target})^{Ct\text{-}target}$. For each condition, the mean MtDNA copy number and the associated standard error (n = 3) were determined. The measured amplification efficiencies were 1.99 and 1.95 *TFB1*and *COX2* genes, respectively. The gene-specific primers used for real time RT-PCR assays in yeast are:

Gene	Accession #	Direction	Sequence
TFC6	NM_001180670.1	Forward primer	5'-GCTCCCCAGGGTCAAGTCTA-3'
		Reverse primer	5'-GCCAGTGGATACCTCTGCAT-3'
TFB1	NM_001180619.3	Forward primer	5'-CGGTGGCTTCATCGGAAAAC-3'
		Reverse primer	5'-TTGCCTCGTACAACTGGGTC-3'
RMD8	NM_001180013.1	Forward primer	5'-GGCCGCTGGATGAACAAGAT-3'
		Reverse primer	5'-TCCCTCATTGCCACGTACAG-3'
COX2	NC_027264.1	Forward primer	5'-TGGTGAAACTGTTGAATTTGAATC-3'
		Reverse primer	5'-CATGACCTGTCCCACACAAC-3'
ATP8	NC_027264.1	Forward primer	5'-ATGCCACAATTAGTTCCATTTTATT-3'
		Reverse primer	5'-CTAGATACATATAATCTTAAGATCATAGGT-3'

2.5. Miscellaneous Procedures.

For mitochondrial enzyme assays and membrane potential analyses, mitochondria were prepared by the enzymatic method [25] from cells grown until middle exponential phase (3-4 x 10^7 cells/mL) in rich galactose medium. Previously described procedures were used to measure oxygen consumption and ATP synthesis rates [26], and mitochondrial ATPase activity [27]. Variations in transmembrane potential ($\Delta\Psi$) were evaluated using Rhodamine 123 with a SAFAS Monaco fluorescence spectrophotometer as described [28]. SDS- BN-PAGE analyses were performed according to [29, 30]. Polyclonal antibodies against Atp6 and Atp9 were used after 1:10.000 dilution, and those against Cox2 (from Molecular Probes) were diluted 1:5.000. Peroxidase-labeled antibodies at 1:10.000 dilution and the ECL reagent of Amersham International were used to reveal proteins probed by the primary antibodies.

2.6. Amino-acid alignments and topology of subunit a mutations.

Multiple sequence alignment of *a*-subunits of various origins was performed using Clustal Omega [31]. The topology of the mutations is based on atomic structures of yeast F_O [7, 21]. Geometry Minimization of the Phenix software suite [32] was used to regularize geometries of the models, with 500 iterations and 5 macro cycles. The shown figures were drawn using PyMOL molecular graphic system [33] and UCSF ChimeraX [34].

2.7. Statistical analysis

At least three biological and three technical replicates were performed for all experiments. The t-test was used for all data sets. Significance and confidence level was set at 0.05.

3. Results

3.1. Isolation of revertants from the $aW_{126}R$ mutant

Yeast subunit *a* is synthesized as a pre-protein of which the first N-terminal residues are removed during assembly of ATP synthase [35-37]. The tryptophan residue at position 109 of human subunit *a* that is changed into arginine by the m.8851T>C mutation corresponds to aW_{126} in the yeast mature protein. One nucleotide change was introduced at codon 136 ($TGA_{136}AGA$) to convert this tryptophan residue into arginine ($aW_{126}R$) [15]. As reported [15], the $aW_{126}R$ mutation severely impairs the growth of yeast on non-fermentable substrates (e.g. glycerol, ethanol) at both 28°C (see Fig. 1) and 36°C owing to defects in the functioning of ATP synthase. Revertants having recovered a good respiratory growth were isolated from forty subclones of the $aW_{126}R$ mutant, to ensure genetic independence of the rescuing mutational alleles (see Materials and Methods). 10^8 cells from each subclone grown in rich 10% glucose were spread on glycerol plates and incubated for two weeks at 28°C. Revertants emerged at a 10^{-7} frequency (an average of ten isolates per plate). The gene *ATP6* was entirely sequenced in thirty-two revertants. Three first-site reversions leading to novel amino acid residues at position 126 were identified: $AGA_{136}ATA$ ($aR_{126}M$) in two clones, $AGA_{136}GGA$ ($aR_{126}G$) in one clone, and $AGA_{136}AAA$ ($aR_{126}K$) in two clones (Table 1). Henceforth, these reversions will be designated as $aW_{126}M$ (instead of $aR_{126}M$), $aW_{126}G$ and $aW_{126}K$, to indicate the amino-acid changes relative to the wild type subunit *a* primary sequence. A second-site suppressor, $AGA_{179}ATA$ ($aR_{169}M$), was also identified, in four clones. As shown in Fig. 1, representatives of these four revertant strains grew in respiratory medium almost like wild type yeast.

No genetic reversion was identified in the *ATP6* gene of the remaining twenty-three sequenced clones. Respiratory competence was preserved after crossing these clones on a minimal glucose medium (W0) to a strain (D273-10B/60) having a wild type nucleus and totally devoid of mitochondrial DNA (ρ^o), which indicated that the suppressors had a mitochondrial origin or were nuclear dominant. The diploid revertant strains were sporulated and respiratory competence segregation in at least six complete tetrads was assessed. In all cases, only 2 spores produced respiratory competent progenies, showing that the suppressors were located in nuclear DNA at a single genetic locus. We didn't analyze further these revertants in the present study.

3.2. Oxidative phosphorylation and mitochondrial membrane potential in the revertants

As we reported [15], the $aW_{126}R$ mutant has a reduced oxidative phosphorylation capacity especially when grown at 36°C with a 90% drop in ATP production relative to the *WT* (60% at 28°C) (Table 2). The mutated ATP synthase accumulates well and assembly intermediates were not detected in BN-gel. The only anomaly is a diminished ratio between F_1F_O dimers and monomers, especially at elevated temperature where this effect is very pronounced ([15], Fig. 2A). However, formation of cristae -a process that requires ATP synthase dimerization [30]- was not found compromised in the mutant [15]. Possibly the mutated ATP synthase keeps *in vivo* the capacity to form dimers but these are fragile and dissociate when subjected to BN-PAGE analysis.

As usually observed in yeast ATP synthase defective mutants [12, 15, 38-41], mitochondria from the $aW_{126}R$ mutant have a diminished content in respiratory complexes, mostly the complex IV ([15], Fig. 2B). Possibly, as discussed [40, 42, 43], complex IV biogenesis is in yeast modulated by the proton transport activity of F_O *via* the transmembrane potential ($\Delta\Psi$) as means to balance electron transfer and ATP synthesis activities. Consistently, complex IV accumulation was not found diminished in yeast ATP synthase mutants with proton leaks through the F_O [44-46].

We biochemically evaluated the rescuing activity of the suppressors in mitochondria isolated from cells grown at 28 or 36°C in a rich galactose medium, in exactly the same conditions used previously to investigate the consequences of the $aW_{126}R$ mutation [15]. The electron transfer to oxygen activity was measured using NADH, alone (state 4), after a further addition (75 μM) of ADP (state 3) and in the presence of the proton ionophore carbonyl cyanide *m*-chlorophenylhydrazone (CCCP) (uncoupled, maximal respiration). Ascorbate/TMPD was used to probe complex IV's activity in isolation. ATP synthesis coupled to NADH oxidation was assayed in the presence of a large excess of external ADP (750 μM). We additionally monitored changes in the transmembrane electrical potential induced by ethanol and ADP, and evaluated the amounts of complexes III, IV and V by BN- and SDS-PAGE. The previously reported data relative to the $aW_{126}R$ and *WT* strains are here included for comparison with the revertants.

3.2.1 In mitochondria from cells grown at 28°C

In the conditions used and with Cox2 antibodies, the complexes III and IV from *WT* mitochondria were detected in BN-gels mainly as III_2-IV_2 and III_2-IV_1 oligomers, with the former being more abundant than the latter (Fig. 2B). In $aW_{126}R$ samples, the complexes III dimers associated with one complex IV (III_2-IV_1) were less abundant (40% *vs WT*) whereas those with two complexes IV (III_2-IV_2) almost normally accumulated. Mitochondria from $aW_{126}K$, $aW_{126}G$, and $aW_{126}M$ strains had a higher content in III_2-IV_2 (60% to >90%) than $aW_{126}R$ and did not show any decrease in III_2-IV_1, whereas both oligomers were in reduced amounts in $aW_{126}R$ + $aR_{169}M$ (30% and 75%, respectively) (Fig. 2B). Complex V was resolved mainly as dimers and monomers (Fig. 2A). From the gels stained with Coomassie blue, it appeared that it was in similar amounts (80-100%) in the analyzed strains except in $aW_{126}R$ + $aR_{169}M$ strain where a substantial decrease (50%) was observed presumably because of a less efficient assembly/stability as indicated by the presence in BN-gels of free subunit *c*-ring as revealed by Western blotting with subunit *c* (Atp9) antibodies (Fig. 2A). Consistently, mitochondria from the $aW_{126}K$, $aW_{126}G$, and $aW_{126}M$ strains respired and produced ATP more efficiently than the original $aW_{126}K$ strain, whereas these activities were not improved by the second-site suppressor mutation $aR_{169}M$ (Table2). However, since the $aW_{126}R$ + $aR_{169}M$ strain has a reduced content in fully assembled ATP synthase compared to $aW_{126}R$, it can be inferred that with the $aR_{169}M$ change the $aW_{126}R$ one has less detrimental consequences on the ATP synthesis activity of F_1F_O molecules (in cells grown at 28°C). With a similar ATP synthesis and P/O values the $aW_{126}R$ and $aW_{126}R$ + $aR_{169}M$ strains should grow similarly at 28°C, which is not the case: the double mutant grows better than the single one (Fig. 1). This apparent discrepancy is addressed below.

We further characterized the influence of the suppressor mutations on oxidative phosphorylation by monitoring changes in transmembrane electrical potential. The mitochondria were first fed with electrons from ethanol, which induced an important fluorescence quenching of Rhodamine 123 in all tested samples (Fig. 3A). This quenching sharply decreases upon a subsequent addition of ADP due $\Delta\Psi$ consumption by the electrogenic exchange of external ADP against matrix-localized ATP, followed by a progressive recovery until most of the added ADP had been transformed

into ATP. Consistent with the ATP synthesis assays (see above), the mitochondria with the $aW_{126}R$ change, alone or in combination with $aR_{169}M$, took a longer time to recover the membrane potential established before the addition of ADP in comparison to those isolated from the other tested strains. As expected, further additions of KCN and CCCP resulted in a total collapse of $\Delta\Psi$ in all samples.

3.2.2. In mitochondria from cells grown at 36°C.

In comparison to mitochondria from the $aW_{126}R$ strain, the rates of ATP synthesis and respiration were several fold increased by all four suppressor mutations (Table 2), ATP synthase recovered a better capacity to form dimers (Fig. 2A), oligomers of complexes III and IV were more abundant (Fig. 2B), and the genetically suppressed mitochondria responded much better to ADP in membrane potential analyses (Fig.3A). The $aR_{169}M$ suppressor had less detrimental consequences on the assembly/stability of ATP synthase (Fig. 2A), which likely explains its better suppressor activity at 36°C compared to 28°C (Table 2). Despite their beneficial effects, the level of oxidative phosphorylation was substantially diminished with the suppressors in comparison to the *WT*. This indicates that the aW_{126} and aR_{169} residues are important to optimize the functioning of ATP synthase especially at elevated temperature, consistent with their good evolutionary conservation (see below).

3.2.2. Influence of the genetic suppressors on the reverse functioning of ATP synthase

The ATP synthase can function reversibly, which is of vital importance in *S. cerevisiae* to maintain an electrical potential across the mitochondrial inner membrane in the absence of oxygen [47]. An easy way to assay ATP synthase reversibility is to measure the rate of ATP hydrolysis in non-osmotically protected mitochondria buffered at pH 8.5, conditions under which this activity is maximal. A large part (85-90%) of it is normally mediated by the F_1 (the main mitochondrial ATPase), and when F_1 and F_O are properly associated to each other this activity is inhibited by oligomycin because blocking subunit *c*-ring rotation prevents rotation of the central stalk and hence ATP processing in F_1. As reported [15], oligomycin-sensitive ATP hydrolysis was considerably decreased by the $aW_{126}R$ mutation (10-15% *vs* the *WT*) both at 28°C and 36°C, whereas it was improved (up to 87%) in the revertants (Table 2).

We further evaluated the influence of the suppressors on the reverse functioning of ATP synthase by monitoring ATP-induced ΔΨ changes in osmotically-protected mitochondria buffered at pH 6.8. The mitochondria were first fed with electrons from ethanol and ΔΨ was subsequently collapsed with KCN to remove from F_1-ATPase its natural inhibitory peptide (IF1), and less than one minute later, well before rebinding of IF_1 [48], ATP was added. The ATP is counter-exchanged against ADP present in the matrix and can then be hydrolyzed in F_1 coupled to F_O-mediated proton transport from the matrix to the IMS. Against a proton gradient the F_1F_O complex functions slowly, which explains that despite their very poor F_1-mediated ATP hydrolytic activity the mitochondria from the *a*W_{126}R strain showed a significant ΔΨ variation in response to ATP albeit of smaller amplitude compared to the *WT* ([15], Fig. 3B). ATP induced a larger and more stable fluorescence variation in mitochondria from the revertants, which further illustrates the beneficial effects of the suppressor mutations on the functioning of ATP synthase.

3.3 Mitochondrial protein and DNA abundance in cells grown at 28°C

As described above, mitochondria from *a*W_{126}R and *a*W_{126}R + *a*R_{169}M cells grown at 28°C have similar ATP synthesis rate (40% *vs* WT) and P/O values (0.7 *vs* 1.1). Somewhat intriguingly while the former showed a very poor growth on glycerol the latter grew much better (Fig.1). Previous studies of numerous yeast ATP synthase mutants have revealed, without any exception, that the activity of this enzyme (measured in isolated mitochondria) needs to be reduced by 80% to see obvious respiratory growth defects [14, 49], and it is thus surprising that the respiratory growth of the *a*W_{126}R strain was so severely compromised at 28°C.

We hypothesized that for some reason *a*W_{126}R cells have a reduced content in mitochondria. To test this hypothesis, we performed several experiments. We first used the DNA-binding 4',6-diamidino-2-phenylindole (DAPI) and mitochondrial potential sensitive MitoTracker-Red CMXRos fluorochromes to visualize nuclear and mitochondrial DNA and the mitochondrial network in log-phase cells after 8h of culture in YPGalA at 28°C. Consistent with their good bioenergetics properties (see above), mitochondria in the three first-site revertants (*a*W_{126}K, *a*W_{126}G and *a*W_{126}M) showed a well-defined tubular organisation as in the *WT*, whereas the mitochondrial network was somewhat

fragmented in the original mutant (*a*W_{126}R) and its second-site revertant (*a*W_{126}R + *a*R_{169}M) possibly reflecting their inability to express mitochondrial function properly (Fig. 4A) (see [50, 51] for reviews on the links between mitochondrial structure and bioenergetics). There was no apparent indication for a reduction in number in the MtDNA nucleoids in the mutant strains compared to *WT* (Fig. 4A). We further probed by Western blot the cellular content in porin (Por1), a protein of the mitochondrial outer membrane, with the cytosolic protein Ade13 as a reference. No significant difference in the content in Por1 was observed between the analyzed strains (Fig. 4B). We additionally determined the mitochondrial DNA copy number per cell by RT-qPCR using primers specific to the nuclear *TFB1* and mitochondrial *COX2* genes (Fig. 4C). Consistent with previous studies [52], we estimated to about 60 the number of mtDNA molecules in the *WT*, and a similar number was scored in the three first-site revertants (*a*W_{126}K, *a*W_{126}G and *a*W_{126}M). Despite their alteration in mitochondrial function, the *a*W_{126}R and W_{126}R + R_{169}M strains did not show a reduced content in mitochondrial DNA but a significant 28% increase. We finally estimated the cellular content in *COX2* and *ATP8* transcripts by RT-qPCR. There was no significant difference in *COX2* transcripts between strains, and any of the mutants showed a diminished abundance in *ATP8* transcripts relative to the *WT* (Fig.4D).

Taken together, these data preclude that a diminished content of mitochondria in cells and defects in mitochondrial gene expression are responsible for the slow growth phenotype on glycerol of the *a*W_{126}R strain despite an ATP synthesis rate in isolated mitochondria (40% *vs WT*) well above the threshold value (20%) below which only respiratory growth is normally compromised. At this stage, the sole theoretical explanation we can offer is that the functioning of ATP synthase in *a*W_{126}R cells is more affected than it is in the assays performed with isolated mitochondria. In these assays, the mitochondria are supplied with large quantities of external ADP to expel rapidly outside the organelle newly synthesized ATP so as to provide the ATP synthase with the highest possible concentration of ADP during the whole course of the experiment. *In vivo*, with possibly a lesser availability in ADP inside the organelle, the rate of ATP synthesis might be less rapid. Whether the strongly reduced capacity of the F_1 to hydrolyze ATP in the *a*W_{126}R -an effect never observed in the thus far studied yeast *atp6* mutants- is in some way involved in the unusual behaviour of this mutant is an interesting hypothesis.

3.4. How the $aW_{126}R$ mutation compromises the functioning of F_O

Within the F_O, two hydrophilic clefts connect the two sides of the membrane with the contact zone between the subunit *c*–ring and subunit *a* [5]. During ATP synthesis, protons from the inter-membrane space are transferred to a glutamate residue in subunit *c* (cE_{59}) in the cleft on the *p*-side of the membrane and are released into the *n*-side cleft after an almost complete rotation of the ring [3-5, 7, 8, 21, 53] (Fig. 5B). The deprotonated subunit *c* monomers are then moved into the *p*-side cleft for a novel loading with protons, which requires an universally conserved arginine residue in subunit *a* (aR_{176} in yeast) located on a bended helical segment (*a*H5) that runs along the *c*-ring. The acidic residues aE_{162} and aD_{244} were recently proposed to be important for the exit of protons from the ring and their transport into the mitochondrial matrix [7, 21].

The tryptophan residue of subunit *a* targeted by the m.8851T>C mutation (aW_{109} in humans, aW_{126} in yeast) is well conserved or replaced by hydrophobic residues (F, L, or V in *A.t.*, *S.p.* and *P.a.* respectively) (Fig. 5A). In the cryo-EM structures of the *S.c.* F_1F_O ATP synthase [7, 21], aW_{126} localizes between helices *a*H4 and *a*H5 at the bottom of the *n*-side cleft near the middle of the membrane (Fig. 4B right panel and E). Its aromatic ring orients towards the *p*-side lipid layer while the indole nitrogen group points into the *n*-side cleft where it forms a hydrogen bond with the carbonyl group of aY_{166} (Fig. 5B right panel). Furthermore aW_{126} and aY_{166} establish a T-shape π-π interaction, which possibly contributes to stabilize the kinked shape of helix *a*H5 (Fig. 4C,D). This topology of aW_{126} fits with the well-known importance of tryptophan in structure and function of membrane proteins with a frequent localization at membrane interfaces [54, 55].

In our structural modeling of the $aW_{126}R$ change induced by the m.8851T>C mutation the aliphatic moieties of aW_{126} and aR_{126} largely overlap at the interface of the *n*-side cleft and membrane lipids while the positively charged guanidinium group of aR_{126} fully localizes inside the hydrophilic interior of the cleft. aR_{126} comes close to the arginine residue aR_{169} (Q_{152} in humans) positioned in the center of the cleft (Fig. 4C). As a result, an electrostatic and steric hindrance displaces aR_{169} towards the ac_{10} interface between aR_{176} and cE_{59} (Fig. 4C). In this orientation, aR_{169} possibly forms a salt bridge with cE_{59} in the F_O rotational 'ground state' as observed in the cryo-EM density map of the *WT*

yeast ATP synthase [21]. Consequently, the structural shift of aR_{169} prevents aR_{176} to interact properly with cE_{59} and proton movements within the F_O and rotation of subunit *c*-ring are impaired, and this explained the lack in ATP synthesis and hydrolysis in mitochondria of the $aW_{126}R$ mutant.

With the $aW_{126}M$ and $aW_{126}G$ suppressors the detrimental electrostatic repulsion between aR_{169} and aR_{126} is eliminated, and local hydrophobicity at the original mutated site is restored with aM_{126} or likely with rotation of the aF_{167} side chain in the gap resulting from the presence of a glycine residue at position 126 (Fig. 4D). While a positive charge remains at position 126 with the $aR_{126}K$ suppressor, the ammonium group of lysine can easily make a hydrogen bond with the main carbonyl chain of aY_{166}, which keeps away aR_{169} from the *c*-ring (Fig. 4E). The second-site suppressor $aR_{169}M$ (Fig. 4F) further strongly supports our proposal that aR_{169} is responsible for the F_O deficiency in the $aW_{126}R$ mutant because of unfavorable interactions with aR_{176} and/or cE_{59}. Although the $aR_{169}M$ change makes the presence of an arginine residue at position 126 less detrimental, the assembly/stability of subunit *a* was found partially compromised in the double mutant whereas alone the $aW_{126}R$ mutation had no impact on ATP synthase formation and accumulation. This indicates that aR_{169} has in its native conformation a role in stabilizing the *n*-side cleft.

Conclusion

We previously showed that the tryptophan to arginine change in subunit *a* induced by the pathogenic m.8851T>C mutation ($aW_{109}R$ in humans, $aW_{126}R$ in yeast) impairs the activity of yeast F_O without any visible assembly defects and proton leaks through the mitochondrial inner membrane [15]. In light of recently described high-resolution structures of yeast ATP synthase [7, 21], the present suppressor genetics analysis affords a molecular explanation for the detrimental consequences of this mutation in yeast. We provide evidence that it does not directly impairs the functioning of F_O, it does so by inducing an electrostatic repulsion and steric hindrance with an arginine residue (aR_{169}) located in the center of the *n*-side cleft along which protons are moved between the *c*-ring and the mitochondrial matrix. As a result, aR_{169} is displaced towards the two residues (aR_{176} and cE_{59}) known for a long time to be essential to the activity and of F_O prevent these residues to function properly.

If the aW_{126} residue is likely not directly involved in the transport of protons across the mitochondrial inner membrane, the suppressor amino acid residues found at position 126 (methionine, glycine, and lysine) only partially restored oxidative phosphorylation especially when yeast was grown at 36°C. As with these residues ATP synthase assembled and accumulated well and the yield in ATP per electron transferred to oxygen was not strongly affected, it can be inferred that the presence of a tryptophan residue at position 126 of subunit *a* optimizes the functioning of yeast F_O, consistent with its good evolutionary conservation. Additionally, our study reveals that aR_{169} has a role in stabilizing the *n*-side cleft. These findings highlight the functional importance of the immediate molecular environment of the regions of subunit *a* that are directly involved in proton transport across the mitochondrial membrane.

Although yeast aR_{169} is conserved in a large number of evolutionary distant species, it is replaced with an electrically neutral glutamine residue in humans (aQ_{152}) (Fig. 5A). aQ_{152} cannot electrostatically trap the essential acidic residue of subunit *c* (cE_{58} in humans) but can impair its interaction with the essential arginine residue of subunit *a* (aR_{159}). At the very least our study demonstrates that the neuromuscular disorders induced by the m.8851T>C mutation result from a failure in the transport of protons between the subunit *c*-ring and the mitochondrial matrix.

Acknowledgements

R.K. was supported by a post-doc fellowship the ANR (Agence Nationale de la Recherche) in J.P.dR.'s lab. K.G. was supported by a post-doc fellowship from the Conseil de la Région Aquitaine. This work was supported by grants from National Science Center of Poland (2016/23/B/NZ3/02098) to R.K., AFM (Association Française contre les Myopathies) to J.-P.dR and D.T.T., and Agence Nationale de la Recherche to A.D. (ANR-12-BSV8-024).

Author Contributions

R.K. and F.G. isolated, sequenced and investigated the biochemical properties of the revertants. A.D. performed the structural modeling analyses. K.G performed the experiments described in figure 4. All authors analyzed the data and contributed to the writing of the manuscript. J.-P.dR. designed the research.

Legends to figures

Figure 1. *Growth phenotypes*. Fresh 28 °C glucose cultures of the indicated strains were serially diluted and 5 µl of each dilution were dropped on rich glycerol and glucose media. The shown plates were incubated at 28°C or 36°C for 5 days.

Figure 2. *ATP synthase and respiratory chain complexes*. Mitochondria isolated from yeast strains grown at 28°C and 36°C were solubilized with digitonin (2 g/g protein) and 200 µg of proteins were separated by BN-PAGE in gels containing a 3–10% polyacrylamide gradient. (A) ATP synthases were visualized by western blot after their transfer onto PVDF membrane with antibodies against Atp6 (subunit *a*), Atp9 (subunit *c*) or Coomassie blue staining. Dimers (V_2) and monomers (V_1) of ATP synthase, and free subunit *c*-rings are indicated on the left. (B) Complexes III and IV. In the conditions used these complexes are detected as dimers of complex III associated to one (III_2-IV_1) or two complexes IV (III_2-IV_2). These oligomers were revealed by Western blot with antibodies against the Cox2 subunit of complex IV. The gels are representative of two independent experiments. Image-J quantification of the protein complexes is provided.

Figure 3. *Mitochondrial membrane potential*. Variations in mitochondrial $\Delta\Psi$ were monitored by fluorescence quenching of Rhodamine 123 in mitochondria isolated from the indicated strains grown at the indicated temperatures. The tracings in panel (A) show how the mitochondria fed with electrons from ethanol responded to externally added ADP; those in panel (B) reflect ATP-driven proton-pumping by ATP synthase. The additions were 0.5 µg/mL Rhodamine 123, 75 µg/mL mitochondrial proteins (Mito), 10 µL ethanol (EtOH), 75 µM ADP (panel A), 1 mM ATP (panel B), 2 mM potassium cyanide (KCN), 4 µg/mL oligomycin (oligo), and 4 µM carbonyl cyanide-m-chlorophenyl hydrazone (CCCP). The shown tracings are representative of three experiments.

Figure 4 *Mitochondrial protein and DNA abundance in cells grown at 28°C.* (A) Epifluorescence microscopy of nuclear and mitochondrial DNA and the mitochondrial network in log-phase cells after

8h of culture in YPGalA at 28°C, using the DNA-binding 4',6-diamidino-2-phenylindole (DAPI) and mitochondrial potential sensitive MitoTracker-Red CMXRos fluorochromes. For each strain, more than 100 cells were observed. Scale bar, 2µm. (B) Abundance of porin relative to Ade13 in total cellular protein extracts resolved by SDS-PAGE and Western Blot with specific antibodies (mean ± SD; n = 3). (C) Quantification of the copy number of MtDNA per cell in the analyzed strains by RT-qPCR (mean ± SD; n = 3). (D) Expression of the mitochondrial *COX2* and *ATP8* genes relative to three nuclear genes (*TFC6*, *TFB1* and *RMD8*) quantified by RT-qPCR (mean ± SD; n = 3). * Significant difference *vs* WT (*: $p < 0.05$, **: $p < 0.01$, ***: $p < 0.001$). ¤ Significant difference *vs* $W_{126}R$ condition (¤¤¤ : $p < 0.001$).

Figure 5. *How the aW_{126}R mutation compromises proton movements within yeast F_O.* (A) Amino-acid alignments of *a*-subunits segments from various mitochondrial origins comprising helices H4, Hβ and H5. The shown sequences are from *Homo sapiens* (*H.s.*), *Bos taurus* (*B.t.*), *Xenopus laevis* (*X.l.*), *Arabidopsis thaliana* (*A.t.*), *Schizosaccharomyces pombe* (*S.p.*), *Podospora anserina* (*P.a.*), *Yarrowia lipolytica* (*Y.l.*) and *Saccharomyces cerevisiae* (*S.c.*). At the top and bottom of the alignment are numbered the residues of the *H.s.* and mature *S.c.* proteins, respectively. Strictly conserved residues are in white characters on a red background. The essential R_{176} residue is on a blue background while similar residues are in red on a white background with blue frames. Residues 126 and 169 mutated in the here studied yeast strains are on a green background. The secondary structures in the *S.c.* protein above the alignments are according to [7]. (B) View of the subunit *a* and the *c*-ring from the peripheral stalk (left panel) and following a 90° rotation (right panel) with as indicated the pathway along which protons are transported from the intermembrane space to the mitochondrial matrix. The *p*-side and *n*-side clefts that connect the two sides of the membrane with subunit *c*/*a* interface are materialized as free lipid area.. The two residues essential (aR_{176} and cE_{59}) for the activity of F_O, and two others (aD_{244}, aE_{162}) important for the exit of protons from the *n*-side cleft are marked, as well as the two residues (aW_{126} and aR_{169}) mutated in the strains here studied. (C-F). Views from the rotor (C-E), from the IMS (D) and from the matrix (F) of the $aW_{126}R$ (C), $aW_{126}G$ (D), $aW_{126}K$ (E) and double $aW_{126}R$ + $aR_{169}M$ changes (F). Three subunits *c* are display as green tubes with cE_{59} in sticks. The large arrow

materializes the putative proton pathway while the dashed arrows indicated rotamer changes of aR$_{169}$ (C) and aF$_{167}$ (D). Hydrogen bonds are drawn as dashed lines. The aW$_{126}$ side chain is shown as yellow and blue ball-and-stick representations while the mutated side chains are in are in orange sticks but sphere for glycine. The moving side chains are colored in magenta and shown as ball-and-stick representations in aW$_{126}$ while the minimized conformations are in sticks.

.

Table 1.

Intragenic suppressors of the $aW_{126}R$ mutation

Codon change	Amino acid change	Number
Original mutant		
$TGA_{136}AGA$	$aW_{126}R$	-
Intragenic suppressors		
$AGA_{136}ATA$	$aW_{126}M$	2
$AGA_{136}GGA$	$aW_{126}G$	1
$AGA_{136}AAA$	$aW_{126}K$	2
$AGA_{179}ATA$	$aR_{169}M$	4

Table 2A. Mitochondrial respiration

Strain	Growth temp. (°C)	Respiration rates nmol O.min^{-1}.mg^{-1} NADH	NADH +ADP	NADH +CCCP	Asc/TMPD + CCCP
WT*	28	279±17	613±12	1081±107	2013±290
$W_{126}R$*	28	203±60	347±25	762±15	1036±27
$W_{126}M$	28	255±32	517±44	923±163	1153±123
$W_{126}G$	28	334±24	644±36	1134±32	1460±61
$W_{126}K$	28	332±80	638±14	1117±116	1655±82
$W_{126}R+R_{169}M$	28	217±10	304±10	424±37	563±13
WT*	36	128±4	368±6	734±54	1130±10
$W_{126}R$*	36	31±13	55±12	87±7	132±22
$W_{126}M$	36	47±4	117±8	192±8	301±41
$W_{126}G$	36	62±7	146±34	232±37	355±69
$W_{126}K$	36	63±8	170±27	318±45	443±20
$W_{126}R+R_{169}M$	36	52±3	129±7	220±9	319±6

Table 2B. Mitochondrial ATP synthesis/hydrolysis

Strain	Growth temp. (°C)	ATPase activity µmol Pi.min^{-1}.mg^{-1} - oligo	+ oligo	oligo-sentitive (% WT)	ATP synthesis rate nmol Pi.min^{-1}.mg^{-1} - oligo	+ oligo	oligo-sentitive (% WT)	P/O
WT*	28	4.48±0.22	0.67±0.11	100	637±18	15±8.0	100	1.04±0.05
$W_{126}R$*	28	1.12±0.06	0.50±0.01	16±1	261±14	8.6±1.0	40±3	0.75±0.10
$W_{126}M$	28	3.50±0.27	0.50±0.02	79±6	679±22	30±2.0	104±3	1.31±0.17
$W_{126}G$	28	2.96±0.10	0.38±0.04	68±2	727±51	23±0.5	113±10	1.12±0.15
$W_{126}K$	28	1.54±0.01	0.27±0.03	33±1	686±31	13±1.0	108±9	1.07±0.08
$W_{126}R+R_{169}M$	28	1.78±0.11	1.07±0.05	19±2	206±22	15±2.0	31±5	0.68±0.10
WT*	36	3.55±0.35	0.89±0.01	100	460±10	1.4±1.0	459	1.25±0.03
$W_{126}R$*	36	1.02±0.09	0.77±0.13	9±2	41±0.6	9.0±0.3	7±1	0.74±0.21
$W_{126}M$	36	3.33±0.88	1.26±0.50	78±24	261±61	7.6±0.8	55±13	2.20±0.76
$W_{126}G$	36	2.80±0.26	1.02±0.14	67±7	288±50	3.6±3.7	62±11	2.20±1.04
$W_{126}K$	36	3.36±0.35	1.04±0.22	87±10	329±68	6.5±3.4	70±15	1.93±1.30
$W_{126}R+R_{169}M$	36	2.91±0.01	2.12±0.08	30±1	237±30	2.1±0	51±6	1.84±0.36

Mitochondria were isolated from cells grown for 5-6 generations in rich galactose medium (YPGalA) at 28°C. Reaction mixes for assays contained 0.15 mg/mL protein, 4 mM NADH, 150 µM ADP (for respiration assays), 750 µM ADP (for ATP synthesis assays), 12.5 mM ascorbate (Asc), 1.4 mM N,N,N,N,-tetramethyl-p-phenylenediamine (TMPD), 4 µM carbonyl cyanide-m-chlorophenyl hydrazone (CCCP), 3 µg/mL oligomycin (oligo). Respiration and ATP synthesis activities were measured using freshly isolated, osmotically protected mitochondria buffered at pH 6.8. For ATPase assays, mitochondria kept at –80°C were thawed and the reaction performed in absence of osmotic protection at pH 8.4. The values reported are averages of triplicate assays ± standard errors. Activities statistically significant comparing to the control mitochondria are in bold ($p<0.05$).*The data relative to WT and $W_{126}R$ strains have been reported [15]; they are here included for comparison with those obtained with the revertants.

References

[1] M. Saraste, Oxidative phosphorylation at the fin de siècle, Science, 283 (1999) 1488-1493.

[2] P.D. Boyer, The ATP synthase--a splendid molecular machine, Annu Rev Biochem, 66 (1997) 717-749.

[3] E. Morales-Rios, M.G. Montgomery, A.G. Leslie, J.E. Walker, Structure of ATP synthase from Paracoccus denitrificans determined by X-ray crystallography at 4.0 A resolution, Proc Natl Acad Sci U S A, 112 (2015) 13231-13236.

[4] A. Zhou, A. Rohou, D.G. Schep, J.V. Bason, M.G. Montgomery, J.E. Walker, N. Grigorieff, J.L. Rubinstein, Structure and conformational states of the bovine mitochondrial ATP synthase by cryo-EM, Elife, 4 (2015).

[5] M. Allegretti, N. Klusch, D.J. Mills, J. Vonck, W. Kuhlbrandt, K.M. Davies, Horizontal membrane-intrinsic alpha-helices in the stator a-subunit of an F-type ATP synthase, Nature, 521 (2015) 237-240.

[6] I.N. Watt, M.G. Montgomery, M.J. Runswick, A.G. Leslie, J.E. Walker, Bioenergetic cost of making an adenosine triphosphate molecule in animal mitochondria, Proc Natl Acad Sci U S A, 107 (2010) 16823-16827.

[7] H. Guo, S.A. Bueler, J.L. Rubinstein, Atomic model for the dimeric FO region of mitochondrial ATP synthase, Science, 358 (2017) 936-940.

[8] A. Hahn, K. Parey, M. Bublitz, D.J. Mills, V. Zickermann, J. Vonck, W. Kuhlbrandt, T. Meier, Structure of a Complete ATP Synthase Dimer Reveals the Molecular Basis of Inner Mitochondrial Membrane Morphology, Mol Cell, 63 (2016) 445-456.

[9] E. Morales-Rios, I.N. Watt, Q. Zhang, S. Ding, I.M. Fearnley, M.G. Montgomery, M.J. Wakelam, J.E. Walker, Purification, characterization and crystallization of the F-ATPase from Paracoccus denitrificans, Open biology, 5 (2015) 150119.

[10] N. Bonnefoy, T.D. Fox, Genetic transformation of Saccharomyces cerevisiae mitochondria, Methods Cell Biol, 65 (2001) 381-396.

[11] K. Okamoto, P.S. Perlman, R.A. Butow, The sorting of mitochondrial DNA and mitochondrial proteins in zygotes: preferential transmission of mitochondrial DNA to the medial bud, J Cell Biol, 142 (1998) 613-623.

[12] M. Rak, E. Tetaud, S. Duvezin-Caubet, N. Ezkurdia, M. Bietenhader, J. Rytka, J.P. di Rago, A yeast model of the neurogenic ataxia retinitis pigmentosa (NARP) T8993G mutation in the mitochondrial ATP synthase-6 gene, J Biol Chem, 282 (2007) 34039-34047.

[13] A.M. Kabala, J.P. Lasserre, S.H. Ackerman, J.P. di Rago, R. Kucharczyk, Defining the impact on yeast ATP synthase of two pathogenic human mitochondrial DNA mutations, T9185C and T9191C, Biochimie, 100 (2014) 200-206.

[14] R. Kucharczyk, N. Ezkurdia, E. Couplan, V. Procaccio, S.H. Ackerman, M. Blondel, J.P. di Rago, Consequences of the pathogenic T9176C mutation of human mitochondrial DNA on yeast mitochondrial ATP synthase, Biochim Biophys Acta, 1797 (2010) 1105-1112.

[15] R. Kucharczyk, M.F. Giraud, D. Brethes, M. Wysocka-Kapcinska, N. Ezkurdia, B. Salin, J. Velours, N. Camougrand, F. Haraux, J.P. di Rago, Defining the pathogenesis of human mtDNA mutations using a yeast model: the case of T8851C, Int J Biochem Cell Biol, 45 (2013) 130-140.

[16] R. Kucharczyk, M. Rak, J.P. di Rago, Biochemical consequences in yeast of the human mitochondrial DNA 8993T>C mutation in the ATPase6 gene found in NARP/MILS patients, Biochim Biophys Acta, 1793 (2009) 817-824.

[17] R. Kucharczyk, B. Salin, J.P. di Rago, Introducing the human Leigh syndrome mutation T9176G into Saccharomyces cerevisiae mitochondrial DNA leads to severe defects in the

incorporation of Atp6p into the ATP synthase and in the mitochondrial morphology, Hum Mol Genet, 18 (2009) 2889-2898.
[18] S. Wen, K. Niedzwiecka, W. Zhao, S. Xu, S. Liang, X. Zhu, H. Xie, D. Tribouillard-Tanvier, M.F. Giraud, C. Zeng, A. Dautant, R. Kucharczyk, Z. Liu, J.P. di Rago, H. Chen, Identification of G8969>A in mitochondrial ATP6 gene that severely compromises ATP synthase function in a patient with IgA nephropathy, Sci Rep, 6 (2016) 36313.
[19] N. Skoczen, A. Dautant, K. Binko, F. Godard, M. Bouhier, X. Su, J.P. Lasserre, M.F. Giraud, D. Tribouillard-Tanvier, H. Chen, J.P. di Rago, R. Kucharczyk, Molecular basis of diseases caused by the mtDNA mutation m.8969G>A in the subunit a of ATP synthase, Biochimica et biophysica acta. Bioenergetics, 1859 (2018) 602-611.
[20] L. De Meirleir, S. Seneca, W. Lissens, E. Schoentjes, B. Desprechins, Bilateral striatal necrosis with a novel point mutation in the mitochondrial ATPase 6 gene, Pediatr Neurol, 13 (1995) 242-246.
[21] A.P. Srivastava, M. Luo, W. Zhou, J. Symersky, D. Bai, M.G. Chambers, J.D. Faraldo-Gomez, M. Liao, D.M. Mueller, High-resolution cryo-EM analysis of the yeast ATP synthase in a lipid membrane, Science, (2018).
[22] J. Ye, G. Coulouris, I. Zaretskaya, I. Cutcutache, S. Rozen, T.L. Madden, Primer-BLAST: a tool to design target-specific primers for polymerase chain reaction, BMC Bioinformatics, 13 (2012) 134.
[23] S.A. Bustin, V. Benes, J.A. Garson, J. Hellemans, J. Huggett, M. Kubista, R. Mueller, T. Nolan, M.W. Pfaffl, G.L. Shipley, J. Vandesompele, C.T. Wittwer, The MIQE guidelines: minimum information for publication of quantitative real-time PCR experiments, Clin Chem, 55 (2009) 611-622.
[24] V. Venegas, M.C. Halberg, Measurement of mitochondrial DNA copy number, Methods in molecular biology, 837 (2012) 327-335.
[25] B. Guerin, P. Labbe, M. Somlo, Preparation of yeast mitochondria (Saccharomyces cerevisiae) with good P/O and respiratory control ratios, Methods Enzymol, 55 (1979) 149-159.
[26] M. Rigoulet, B. Guerin, Phosphate transport and ATP synthesis in yeast mitochondria: effect of a new inhibitor: the tribenzylphosphate, FEBS Lett, 102 (1979) 18-22.
[27] M. Somlo, Induction and repression of mitochondrial ATPase in yeast, Eur J Biochem, 5 (1968) 276-284.
[28] R.K. Emaus, R. Grunwald, J.J. Lemasters, Rhodamine 123 as a probe of transmembrane potential in isolated rat-liver mitochondria: spectral and metabolic properties, Biochim Biophys Acta, 850 (1986) 436-448.
[29] U.K. Laemmli, Cleavage of structural proteins during the assembly of the head of bacteriophage T4, Nature, 227 (1970) 680-685.
[30] P. Paumard, J. Vaillier, B. Coulary, J. Schaeffer, V. Soubannier, D.M. Mueller, D. Brethes, J.P. di Rago, J. Velours, The ATP synthase is involved in generating mitochondrial cristae morphology, EMBO J, 21 (2002) 221-230.
[31] F. Sievers, A. Wilm, D. Dineen, T.J. Gibson, K. Karplus, W. Li, R. Lopez, H. McWilliam, M. Remmert, J. Soding, J.D. Thompson, D.G. Higgins, Fast, scalable generation of high-quality protein multiple sequence alignments using Clustal Omega, Molecular systems biology, 7 (2011) 539.
[32] P.D. Adams, P.V. Afonine, G. Bunkoczi, V.B. Chen, I.W. Davis, N. Echols, J.J. Headd, L.W. Hung, G.J. Kapral, R.W. Grosse-Kunstleve, A.J. McCoy, N.W. Moriarty, R. Oeffner, R.J. Read, D.C. Richardson, J.S. Richardson, T.C. Terwilliger, P.H. Zwart, PHENIX: a comprehensive Python-based system for macromolecular structure solution, Acta Crystallogr D Biol Crystallogr, 66 (2010) 213-221.
[33] W.L. DeLano, PyMOL molecular graphics system, (2002).

[34] T.D. Goddard, C.C. Huang, E.C. Meng, E.F. Pettersen, G.S. Couch, J.H. Morris, T.E. Ferrin, UCSF ChimeraX: Meeting modern challenges in visualization and analysis, Protein science : a publication of the Protein Society, 27 (2018) 14-25.
[35] T. Michon, M. Galante, J. Velours, NH2-terminal sequence of the isolated yeast ATP synthase subunit 6 reveals post-translational cleavage, Eur J Biochem, 172 (1988) 621-625.
[36] X. Zeng, W. Neupert, A. Tzagoloff, The metalloprotease encoded by ATP23 has a dual function in processing and assembly of subunit 6 of mitochondrial ATPase, Mol Biol Cell, 18 (2007) 617-626.
[37] C. Osman, C. Wilmes, T. Tatsuta, T. Langer, Prohibitins interact genetically with Atp23, a novel processing peptidase and chaperone for the F1Fo-ATP synthase, Mol Biol Cell, 18 (2007) 627-635.
[38] S. Marzuki, L.C. Watkins, W.M. Choo, Mitochondrial H+-ATPase in mutants of Saccharomyces cerevisiae with defective subunit 8 of the enzyme complex, Biochim Biophys Acta, 975 (1989) 222-230.
[39] M.F. Paul, J. Velours, G. Arselin de Chateaubodeau, M. Aigle, B. Guerin, The role of subunit 4, a nuclear-encoded protein of the F0 sector of yeast mitochondrial ATP synthase, in the assembly of the whole complex, Eur J Biochem, 185 (1989) 163-171.
[40] M. Rak, E. Tetaud, F. Godard, I. Sagot, B. Salin, S. Duvezin-Caubet, P.P. Slonimski, J. Rytka, J.P. di Rago, Yeast cells lacking the mitochondrial gene encoding the ATP synthase subunit 6 exhibit a selective loss of complex IV and unusual mitochondrial morphology, J Biol Chem, 282 (2007) 10853-10864.
[41] M.J.B. Jean-Francois, H.B. Lukins, S. Marzuki, Post-transcriptional defects in the synthesis of the mitochondrial H +-ATPase
subunit 6 in yeast mutants with lesions in the subunit 9 structural gene, Biochimica et Biophysica Acta, 868 (1986) 178-182.
[42] I.C. Soto, F. Fontanesi, M. Valledor, D. Horn, R. Singh, A. Barrientos, Synthesis of cytochrome c oxidase subunit 1 is translationally downregulated in the absence of functional F1F0-ATP synthase, Biochim Biophys Acta, 1793 (2009) 1776-1786.
[43] C. Schwimmer, L. Lefebvre-Legendre, M. Rak, A. Devin, P.P. Slonimski, J.P. di Rago, M. Rigoulet, Increasing mitochondrial substrate-level phosphorylation can rescue respiratory growth of an ATP synthase-deficient yeast, J Biol Chem, 280 (2005) 30751-30759.
[44] Y. Xiao, M. Metzl, D.M. Mueller, Partial uncoupling of the mitochondrial membrane by a heterozygous null mutation in the gene encoding the gamma- or delta-subunit of the yeast mitochondrial ATPase, J Biol Chem, 275 (2000) 6963-6968.
[45] S. Duvezin-Caubet, M. Caron, M.F. Giraud, J. Velours, J.P. di Rago, The two rotor components of yeast mitochondrial ATP synthase are mechanically coupled by subunit delta, Proc Natl Acad Sci U S A, 100 (2003) 13235-13240.
[46] E. Tetaud, F. Godard, M.F. Giraud, S.H. Ackerman, J.P. di Rago, The depletion of F(1) subunit epsilon in yeast leads to an uncoupled respiratory phenotype that is rescued by mutations in the proton-translocating subunits of F(0), Mol Biol Cell, 25 (2014) 791-799.
[47] L. Lefebvre-Legendre, A. Balguerie, S. Duvezin-Caubet, M.F. Giraud, P.P. Slonimski, J.P. Di Rago, F1-catalysed ATP hydrolysis is required for mitochondrial biogenesis in Saccharomyces cerevisiae growing under conditions where it cannot respire, Mol Microbiol, 47 (2003) 1329-1339.
[48] R. Venard, D. Brethes, M.F. Giraud, J. Vaillier, J. Velours, F. Haraux, Investigation of the role and mechanism of IF1 and STF1 proteins, twin inhibitory peptides which interact with the yeast mitochondrial ATP synthase, Biochemistry, 42 (2003) 7626-7636.
[49] A. Mukhopadhyay, M. Uh, D.M. Mueller, Level of ATP synthase activity required for yeast Saccharomyces cerevisiae to grow on glycerol media, FEBS Lett, 343 (1994) 160-164.

[50] G. Benard, R. Rossignol, Ultrastructure of the mitochondrion and its bearing on function and bioenergetics, Antioxidants & redox signaling, 10 (2008) 1313-1342.
[51] C. Sauvanet, S. Duvezin-Caubet, J.P. di Rago, M. Rojo, Energetic requirements and bioenergetic modulation of mitochondrial morphology and dynamics, Semin Cell Dev Biol, 21 (2010) 558-565.
[52] S. Vijayraghavan, S.G. Kozmin, P.K. Strope, D.A. Skelly, Z. Lin, J. Kennell, P.M. Magwene, F.S. Dietrich, J.H. McCusker, Mitochondrial Genome Variation Affects Multiple Respiration and Nonrespiration Phenotypes in Saccharomyces cerevisiae, Genetics, 211 (2019) 773-786.
[53] A. Hahn, J. Vonck, D.J. Mills, T. Meier, W. Kuhlbrandt, Structure, mechanism, and regulation of the chloroplast ATP synthase, Science, 360 (2018).
[54] W.M. Yau, W.C. Wimley, K. Gawrisch, S.H. White, The preference of tryptophan for membrane interfaces, Biochemistry, 37 (1998) 14713-14718.
[55] D.A. Kelkar, A. Chattopadhyay, Membrane interfacial localization of aromatic amino acids and membrane protein function, Journal of biosciences, 31 (2006) 297-302.

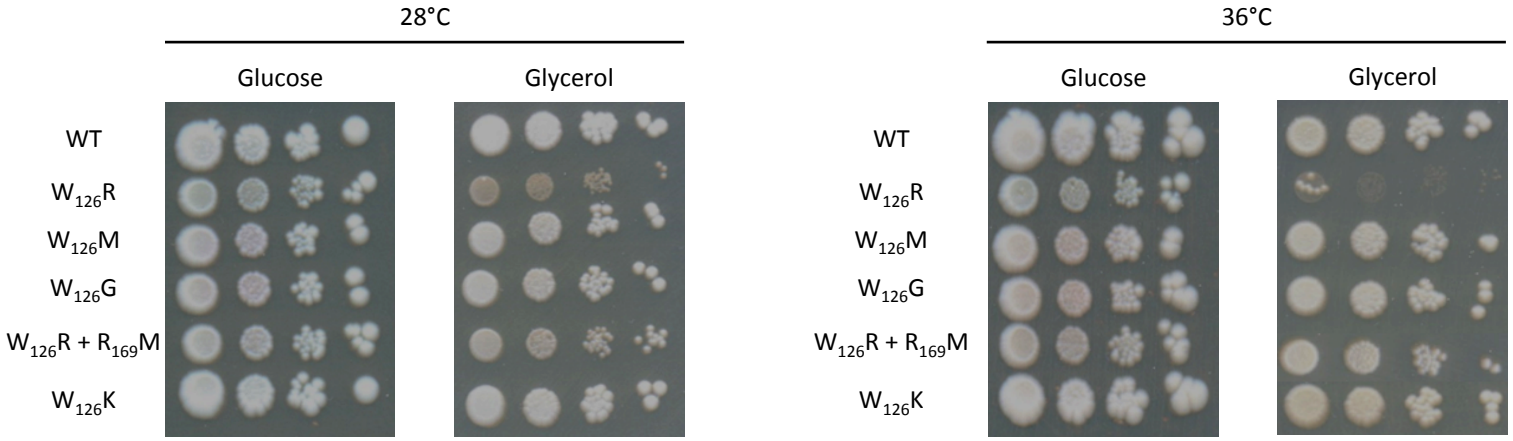
28°C
36°C
Glucose
Glycerol
Glucose
Glycerol
WT
$W_{126}R$
$W_{126}M$
$W_{126}G$
$W_{126}R + R_{169}M$
$W_{126}K$
WT
$W_{126}R$
$W_{126}M$
$W_{126}G$
$W_{126}R + R_{169}M$
$W_{126}K$

A

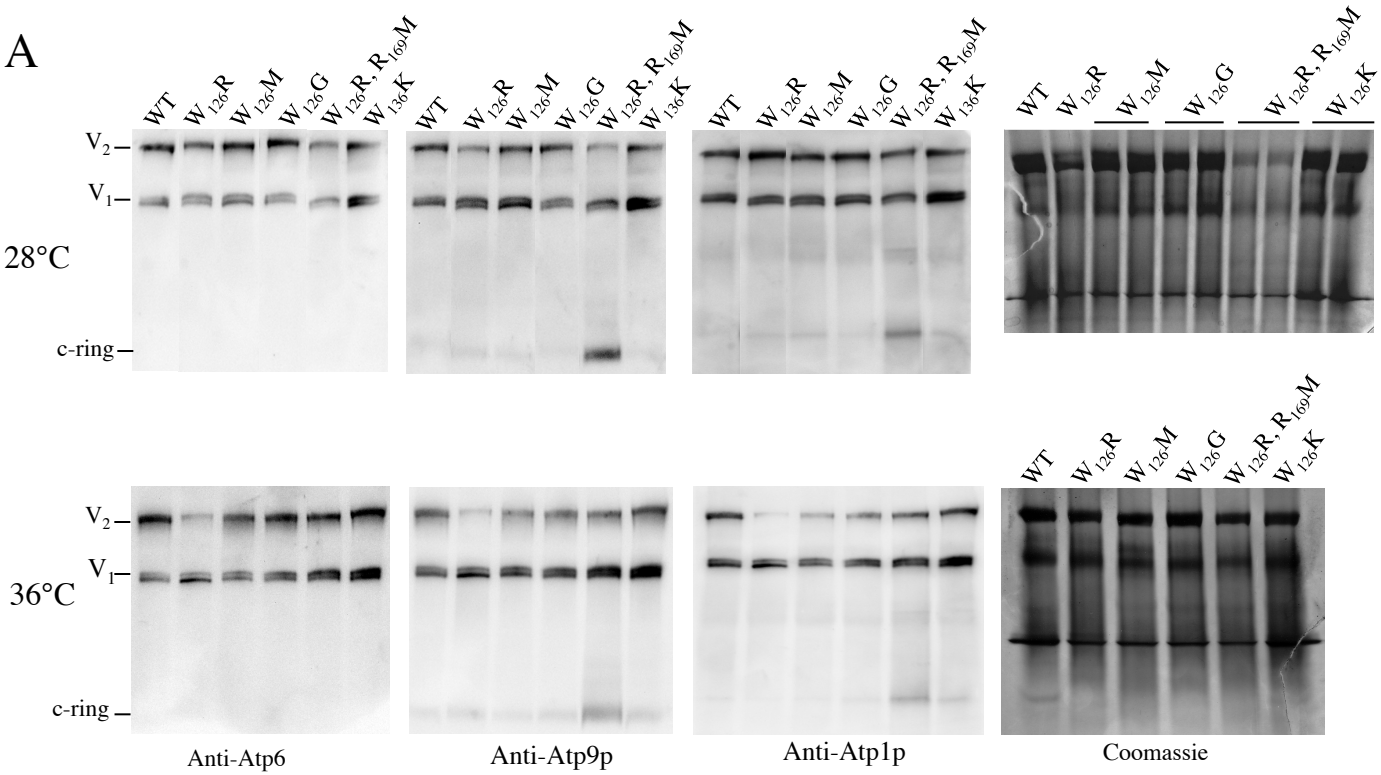

F_1F_O (% WT)

	28°C	36°C
WT	100	100
$W_{126}R$	80	89
$W_{126}M$	87	89
$W_{126}G$	95	94
$W_{126}R$+ $R_{169}M$	50	83
$W_{126}K$	87	95

B

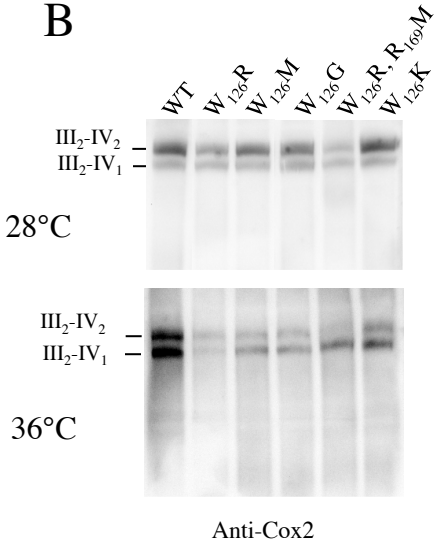

Oligomers of complexes III and IV in % WT						
	WT	W126R	$W_{126}M$	$W_{126}G$	$W_{126}R$ +$R_{169}M$	$W_{126}K$
III_2-IV_2	100	38	60	60	28	96
III_2-IV_1	100	114	118	120	76	115

Oligomers of complexes III and IV in % WT						
	WT	W126R	$W_{126}M$	$W_{126}G$	$W_{126}R$ +$R_{169}M$	$W_{126}K$
III_2-IV_2	100	21	23	24	32	42
III_2-IV_1	100	17	30	29	45	51

Figure 2

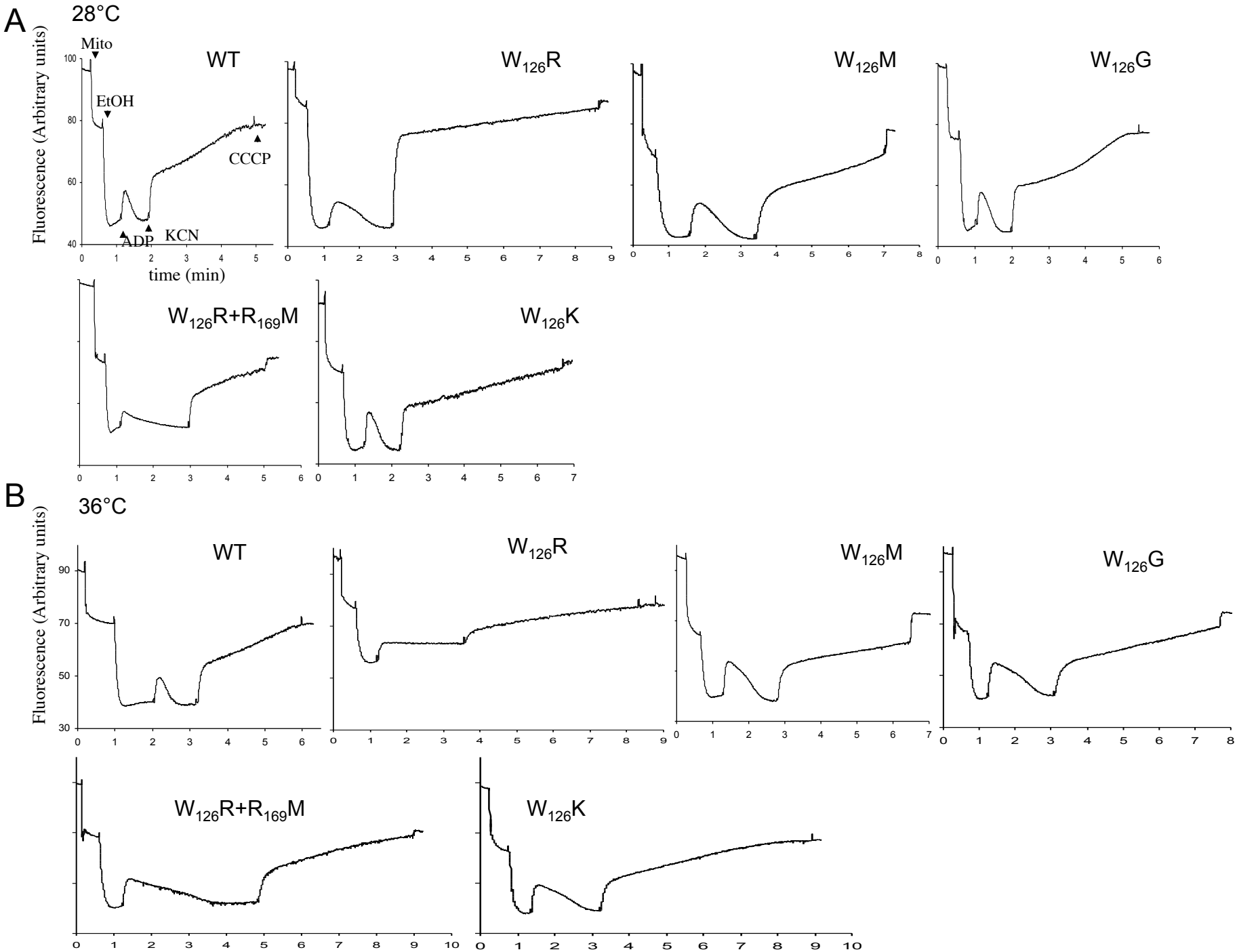
A
28°C
Fluorescence (Arbitrary units)
Mito
EtOH
ADP
KCN
CCCP
time (min)
WT
W126R
W126M
W126G
W126R+R169M
W126K
B
36°C
Fluorescence (Arbitrary units)
WT
W126R
W126M
W126G
W126R+R169M
W126K

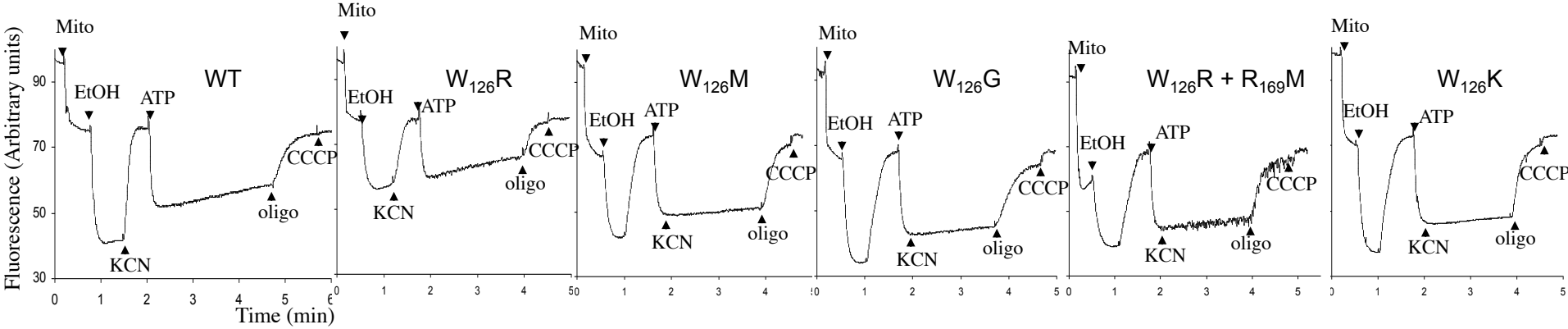
Fluorescence (Arbitrary units)
Time (min)
WT
W126R
W126M
W126G
W126R + R169M
W126K
Mito
EtOH
ATP
KCN
oligo
CCCP

Figure 3B

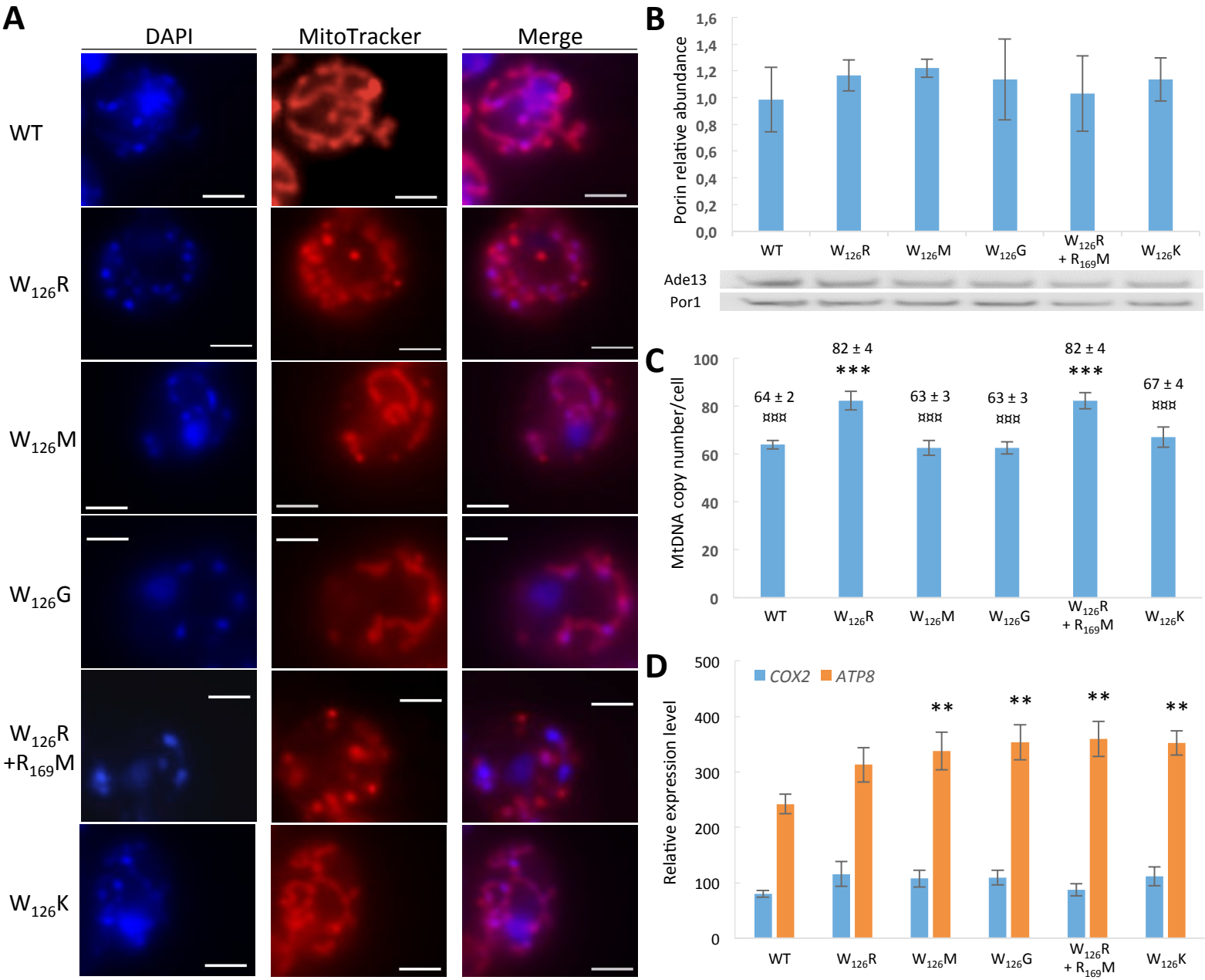
A
DAPI
MitoTracker
Merge
WT
W126R
W126M
W126G
W126R +R169M
W126K
B
Porin relative abundance
1,6
1,4
1,2
1,0
0,8
0,6
0,4
0,2
0,0
WT
W126R
W126M
W126G
W126R + R169M
W126K
Ade13
Por1
C
MtDNA copy number/cell
100
80
60
40
20
0
64 ± 2
¤¤¤
82 ± 4
***
63 ± 3
¤¤¤
63 ± 3
¤¤¤
82 ± 4
***
67 ± 4
¤¤¤
WT
W126R
W126M
W126G
W126R + R169M
W126K
D
Relative expression level
500
400
300
200
100
0
COX2
ATP8
**
**
**
**
WT
W126R
W126M
W126G
W126R + R169M
W126K

Figure 4

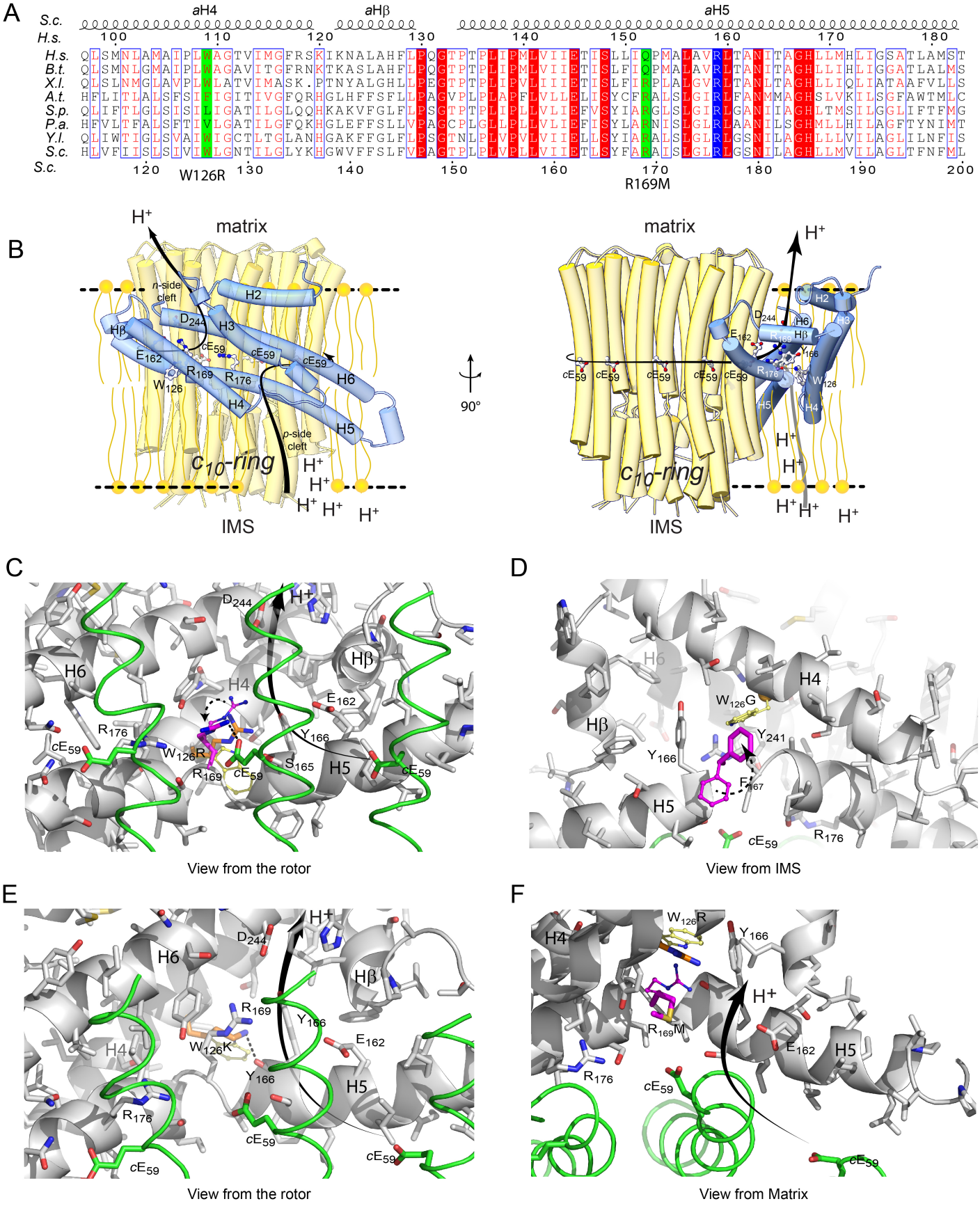
A
aH4
aHβ
aH5
S.c.
H.s.
W126R
R169M
B
matrix
H+
n-side cleft
p-side cleft
H2
H3
Hβ
H4
H5
H6
D244
E162
R169
R176
W126
cE59
c10-ring
IMS
90°
C
View from the rotor
D
View from IMS
E
View from the rotor
F
View from Matrix

Figure 5